Int. J. Solids Structures Vol. 29, No. 4, pp. 421–436, 1992
Printed in Great Britain.

0020–7683/92 $5.00 + .00
Pergamon Press plc

PENETRATION OF LAMINATED KEVLAR BY PROJECTILES—II. ANALYTICAL MODEL

GUOQI ZHU,† WERNER GOLDSMITH and C. K. H. DHARAN
Department of Mechanical Engineering, University of California,
Berkeley, CA 94720, U.S.A.

(*Received* 18 *January* 1991; *in revised form* 11 *June* 1991)

Abstract—An analytical representation of the normal impact and perforation of conically-tipped hard-steel cylinders with an aspect ratio of three on laminated Kevlar 29/polyester targets was developed to accompany corresponding text information. The global deflection was obtained using laminated plate theory; dissipative mechanisms including indentation of the striker tip, bulging at the surface, fiber failure, delamination and friction were modeled using certain simplifying assumptions. The event was divided into three consecutive phases: indentation, perforation and exit. Resistive forces for each of these mechanisms, valid for both static and dynamic penetration, were ascertained and, for the latter case, used in conjunction with Newton's law to provide the plate response and the kinematic history of the projectile. A finite difference scheme was employed to obtain the numerical results.

A comparison of the ballistic limits and of terminal velocities for higher initial speeds obtained from the model and from tests showed very good agreement. The accord between predicted and measured displacement histories is satisfactory, but deteriorates successively when velocities and accelerations are examined. This effect is due to the process of differentiation of data as well as inaccuracies in the analytical representation. Methods for extending the model are suggested.

INTRODUCTION

In a companion paper, Zhu *et al.* (1991), the results of experiments involving the normal penetration and perforation of Kevlar 29/polyester resin laminates by conically-tipped cylindrical hard-steel projectiles were presented. The phenomena involved in the dynamic loading of such plates are complex; a comprehensive analysis of such an event requires consideration of a wide variety of processes, including global deformation, local indentation, bulging, frictional effects and a variety of failure mechanisms. While numerous physical and numerical models of the penetration and perforation of isotropic materials have been published, corresponding work involving composite laminates is much more limited.

Failure mechanisms in these materials due to impact by blunt projectiles were described by Cristescu *et al.* (1975), while Greszczuk (1975) and Greszczuk and Chao (1977) computed the stress distribution and damage for such an event. Low velocity impact of spheres on composites was modeled analytically by Shivakumar *et al.* (1985a,b) who developed a physical model using the Tsai-Wu failure criterion, Tsai and Wu (1971), as well as a maximum stress criterion for damage evaluation. Fiber failure and delamination were attributed to target bending, but local bulging was not considered. Tan and Sun (1985) and Sun (1977) studied the same phenomenon using the Whitney–Pagano laminate theory, Whitney and Pagano (1970), to estimate the global deformation of the laminates and an empirical indentation law, considered to be the same under both static and dynamic conditions, to approximate the contact force. Matrix cracking and delamination were included, but not fiber failure. Computational developments of impact on laminated plates may be found in Cairns and Lagace (1987), Dobyns (1981) and Reddy (1982).

Delamination has been studied using linear elastic fracture mechanics, Dharan (1978), Garg (1988) and Wang (1984). The case of an elliptically-shaped delamination under quasi-static in-plane compression was investigated by Chai (1982), Chai and Babcock (1984) and Flanagan (1988). Ply separation resulting from low velocity impact by a sphere was analyzed by Wu and Springer (1988a,b) and by Grady and Sun (1985) who employed both finite element and experimental techniques.

† Current address: CPC Group, General Motors Corporation, Warren, MI, U.S.A.

This paper is concerned with the construction of a model of the perforation of conically-tipped projectiles into Kevlar laminates involving speeds at and somewhat above the ballistic limit. The penetration phenomenon was divided into three successive and non-interactive stages: (a) indentation, (b) perforation, and (c) exit of the projectile. The predictions of this model have been compared with data from corresponding experiments for a variety of impact conditions.

A finite difference program incorporating the global response, local deformation, and fiber and matrix failure, as well as the motion of the projectile, was developed. The computed results were compared with corresponding experimental data, Zhu *et al.* (1991).

ASSUMPTIONS

The model includes a number of idealizations, such as thin plate behavior, the rigidity of the projectile, the independence of global and local response of the laminate, the enlargement of a spherical cap due to indentation until perforation occurs and the maintenance of a spherical bulge thereafter, fiber deformation in the form of a geodesic around this bulge or around the indenting cone, and the use of a solid friction representation. Since the material is considered to be incompressible, the volume of the bulge is equal to that of the conical penetration. The shape of the delamination is specified as being elliptical which is found for the case of different fiber densities in the two orthogonal directions. The location of the greatest delamination is assumed to occur on the distal side; propagation is mode I dominated. The resistance of the damaged composite is included in the form of a parameter which is the ratio of the number of failed fibers to the total number of unbroken fibers in front of the contact zone.

Matrix cracking, although observed, was found to be minor and was hence neglected in the model. Whitney–Pagano theory, which is linearly elastic and limited to small strains, is also used here for determining the global deflection. Rate effects are incorporated in the analysis by using the value of the dynamic rather than a static yield stress in the equations. The assumed independence of the global and local response of the laminate to dynamic loading leads to the relation between the displacement of the projectile, w_p, as the sum of the central plate deflection, w_c, and the relative indentation (or perforation) of the projectile with respect to the plate, w_r.

GLOBAL RESPONSE

Whitney–Pagano laminated plate theory, which is an extension of the theory of Yang *et al.* (1966), was used in the analysis of the response of composite specimens to impact. The displacement equations of motion are given by

$$A_{11}u^0_{,xx}+2A_{16}u^0_{,xy}+A_{66}u^0_{,yy}+A_{16}v^0_{,xx}+(A_{12}+A_{66})v^0_{,xy}+A_{26}v^0_{,yy}$$
$$+B_{11}\Psi_{x,xx}+2B_{16}\Psi_{x,xy}+B_{66}\Psi_{x,yy}+B_{16}\Psi_{y,xx}+(B_{12}+B_{66})\Psi_{y,xy}$$
$$+B_{26}\Psi_{y,yy}=P\ddot{u}^0+R\ddot{\Psi}_x$$

$$A_{16}u^0_{,xx}+(A_{12}+A_{66})u^0_{,xy}+A_{26}u^0_{,yy}+A_{66}v^0_{,xx}+2A_{26}v^0_{,xy}+A_{22}v^0_{,yy}$$
$$+B_{16}\Psi_{x,xx}+(B_{12}+B_{66})\Psi_{x,xy}+B_{26}\Psi_{x,yy}+B_{66}\Psi_{y,xx}+2B_{26}\Psi_{y,xy}$$
$$+B_{22}\Psi_{y,yy}=P\ddot{v}^0+R\ddot{\Psi}_y$$

$$k[A_{55}(\Psi_{x,x}+w_{,xx})+A_{45}(\Psi_{x,y}+\Psi_{y,x}+2w_{,xy})+A_{44}(\Psi_{y,y}+w_{,yy})]+p=P\ddot{w}$$

$$B_{11}u^0_{,xx}+2B_{16}u^0_{,xy}+B_{66}u^0_{,yy}+B_{16}v^0_{,xx}+(B_{12}+B_{66})v^0_{,xy}+B_{26}v^0_{,yy}$$
$$+D_{11}\Psi_{x,xx}+2D_{16}\Psi_{x,xy}+D_{66}\Psi_{x,yy}+D_{16}\Psi_{y,xx}+(D_{12}+D_{66})\Psi_{y,xy}$$
$$+D_{26}\Psi_{y,yy}-k[A_{55}(\Psi_x+w_{,x})+A_{45}(\Psi_y+w_{,y})]=R\ddot{u}^0+I\ddot{\Psi}_x$$

$$B_{16}u^0_{,xx}+(B_{12}+B_{66})u^0_{,xy}+B_{26}u^0_{,yy}+B_{66}v^0_{,xx}+2B_{26}v^0_{,xy}+B_{22}v^0_{,yy}$$
$$+D_{16}\Psi_{x,xx}+(D_{12}+D_{66})\Psi_{x,xy}+D_{26}\Psi_{x,yy}+D_{66}\Psi_{y,xx}+2D_{26}\Psi_{y,xy}$$
$$+D_{22}\Psi_{y,yy}-k[A_{45}(\Psi_x+w_{,x})+A_{44}(\Psi_y+w_{,y})]=R\ddot{v}^0+I\ddot{\Psi}_y \quad (1)$$

where A_{ij} are the components of the extensional stiffness matrix, B_{ij} are those of the coupled extension–bending matrix and D_{ij} are the elements of the bending stiffness matrix, with $i, j = 1, \ldots, 6$, with certain terms omitted due to the thin plate hypothesis. The displacements in the in-plane (x, y) and transverse directions are u, v and w, respectively, and Ψ_m are the angular displacements, where $m = x, y, z$. Superscript 0 refers to the mid-plane of the laminate, p is the external pressure and k is the Mindlin shear correction factor. Inertial factors P, R and I are defined by

$$(P, R, I) = \int_{-h/2}^{h/2} \rho(1, z, z^2)\,dz \quad (2)$$

where ρ is the mass density. The appropriate initial and boundary conditions to guarantee a unique solution of eqns (1) can be determined from the total energy of the system; in general, five initial and five boundary conditions are required.

LOCAL DAMAGE MODEL

For the present layered composite, the local damage mechanisms due to penetration modeled here are bulging, delamination and fiber deformation and failure; matrix cracking was neglected. The analysis is carried out by determining the total resistive force acting on the projectile due to each of these three processes. This is accomplished by consideration of the three successive stages of indentation, perforation and exit of the projectile. Indentation is characterized totally by local bulging. The experimentally observed initial fiber failure due to the combined effects of global deformation and local damage in plates of 20 plies or fewer, which occurs on the distal side of the target, defines the termination of indentation and the start of perforation.

Perforation is characterized by fiber failure at the ultimate strain value and by delamination as well as the further growth of the bulge. The plate resistance successively decreases as the number of ruptured filaments (and hence the damage parameter) increases. The effect of friction becomes more dominant the greater the embedment of the striker. The initiation of the exit stage occurs upon emergence of the entire conical tip from the target. At this instant, the resistive force drops to the value of the friction force; this force remains constant during the remaining contact period.

(a) *Bulging*

A continuum-mechanical analysis of the bulging process is prohibitive; instead, it is assumed that the bulge forms a spherical cap in accordance with experimental observation, as shown in Fig. 1. A similar assumption has been employed by Awerbuch and Bodner (1970) in the investigation of the bulging of a metallic plate penetrated by a blunt projectile. Conservation of volume is employed in calculating the extent of bulging.

From Fig. 1 the half chord of the bulge, r_2, can be expressed as

$$r_2 = w_r \tan\beta + h \tan\xi \quad (3)$$

where β is the half angle of the cone of the projectile, ξ is the half angle of the sector of a sphere, and h is the thickness of the laminate. The radius of the sphere, r, is given by

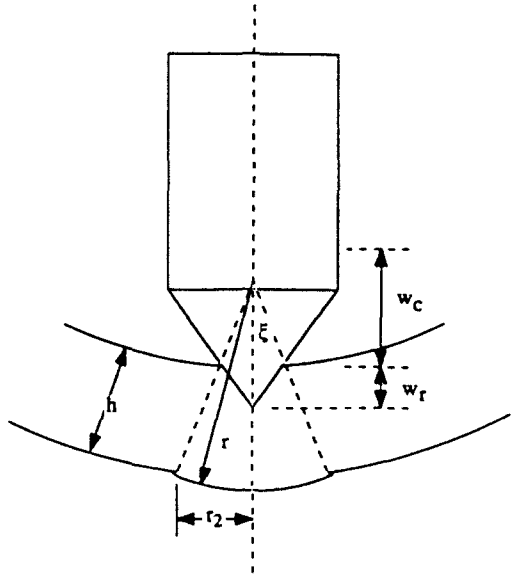

Fig. 1. Idealized model for global displacement and bulging of a laminated plate penetrated normally by a sharp-pointed projectile.

$$r = \frac{r_2}{\sin \xi}. \tag{4}$$

By equating the volume of the cone embedded in the composite at any time to the volume of the bulge, ξ can be calculated from

$$\left(\frac{w_f}{h} \sin \xi\right)^3 \tan^2 \beta - \left(\frac{w_f}{h} \tan \beta + \tan \xi\right)^3 (1 - \cos \xi)^2 (2 + \cos \xi) = 0. \tag{5}$$

The shape of the bulge after fiber failure becomes more complicated, since the broken fibers are free of constraint. It is assumed that the bulge remains spherical and that eqn (5) continues to hold.

(b) *Delamination*

When the projectile enters the target, the material is displaced laterally as well as downward, producing in-plane compression with a highly localized deformation gradient as well as out-of-plane loading. This results in interlaminar cracking of mixed I and II mode type. The reflection of the pressure wave created by the impact generates a tensile wave, which produces incipient Mode I delamination, that is extended by the penetration of the projectile as shown in Fig. 2.

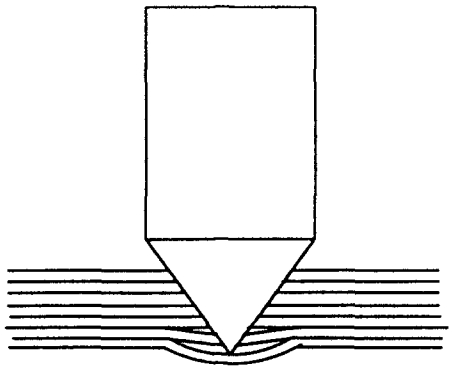

Fig. 2. Delamination initiation during penetration of a laminate by a cylindro-conical projectile.

The maximum delamination is taken to occur on the distal side, a result supported by experimental observation, so that the propagation of the crack is primarily Mode I. Its shape is generally modeled as an ellipse with semi-major axes a and b, respectively, in linear elastic fracture mechanics [i.e. Chai and Babcock (1984)]. This is the starting point in the present analysis even though the actual configuration is more complex due to the variations in stiffness between the weave directions. Furthermore, the weave in the orthogonal directions is identical; thus, the energy release rates in these directions, G_a (along direction a) and G_g (along b) should be identical and the initial delamination circular, a condition for which the final results are computed. The relevant equations are obtained by specialization of the elliptical case, for which the energy release rate G_I can be expressed as, Chai and Babcock (1984),

$$G_I = \frac{G_I^a + G_I^b \dfrac{adb}{bda}}{1 + \dfrac{adb}{bda}}. \tag{6}$$

Here, G_I^a and G_I^b are the energy release rates along the a and b axes, respectively, given by

$$G_I^a = \frac{-1}{\pi b}\frac{\partial U}{\partial a} \tag{7a}$$

$$G_I^b = \frac{-1}{\pi a}\frac{\partial U}{\partial b} \tag{7b}$$

where U is the plate strain energy. The deflection of a circular, isotropic plate, w, at a position of radius r due to a concentrated central force is given by, Timoshenko (1959),

$$w = P\frac{r^2}{8\pi D_h}\log\frac{r}{R} + \frac{P}{16\pi D_h}(R^2 - r^2) \tag{8}$$

where P is the concentrated load, R is the radius of the clamped plate and D_h is the flexural stiffness. Based on this result, for elliptical delamination, the form of the deflection of the sublaminate is assumed as

$$w = w_0\left(1 - \frac{x^2}{a^2} - \frac{y^2}{b^2}\right) + w_0\left(\frac{x^2}{a^2} + \frac{y^2}{b^2}\right)\ln\left(\frac{x^2}{a^2} + \frac{y^2}{b^2}\right) \tag{9}$$

where w_0 is the deflection at the center of the sublaminate and x and y are the coordinates along directions a and b, respectively. Employing Von Karman strain–displacement relations, strain ε and curvature κ are expressed as

$$\varepsilon = (\varepsilon_x, \varepsilon_y, \gamma_{xy}) = \frac{1}{2}\left(\frac{\partial w}{\partial x}\right)^2, \frac{1}{2}\left(\frac{\partial w}{\partial y}\right)^2, \frac{1}{2}\left(\frac{\partial w}{\partial x}\frac{\partial w}{\partial y}\right) \tag{10a}$$

$$\kappa = (\kappa_x, \kappa_y, \kappa_{xy}) = \left(-\frac{\partial^2 w}{\partial x^2}, -\frac{\partial^2 w}{\partial x^2}, -\frac{\partial^2 w}{\partial x\,\partial y}\right) \tag{10b}$$

where subscripts denote the component directions. G_I^a and G_I^b can be obtained after U is computed.

The strain energy of the plate is represented by

$$U = \frac{1}{2}\iint (\varepsilon^t A\varepsilon + 2\kappa^t B\varepsilon + \kappa^t D\kappa)\,dx\,dy \tag{11}$$

where A, B and D are the extensional, coupling and flexural stiffness matrices, respectively, for the sublaminate which can be calculated from the deflection presented in eqn (9).

In the following analysis, the lay-up of the sublaminate is symmetric as is the case here. By substituting eqn (9) into eqn (10), the strain energy is given by

$$U = \frac{2\pi w_0^4 ab}{81}\left[\frac{6A_{11}}{a^4} + \frac{6A_{22}}{b^4} + \frac{A_{66}+2A_{12}}{a^2b^2}\right] + \pi w_0^2 ab\left[\frac{6D_{11}}{a^4} + \frac{6D_{22}}{b^4} + \frac{D_{66}+2D_{12}}{a^2b^2}\right]. \tag{12}$$

Therefore, G^a and G^b can be expressed as

$$G^a = -\frac{1}{\pi b}\frac{\partial U}{\partial a} = \frac{2w_0^4}{81}\left[\frac{18A_{11}}{a^4} - \frac{6A_{22}}{b^4} + \frac{A_{66}+2A_{12}}{a^2b^2}\right] + w_0^2\left[\frac{18D_{11}}{a^4} - \frac{6D_{22}}{b^4} + \frac{D_{66}+2D_{12}}{a^2b^2}\right] \tag{13a}$$

$$G^b = -\frac{1}{\pi a}\frac{\partial U}{\partial b} = \frac{2w_0^4}{81}\left[-\frac{6A_{11}}{a^4} + \frac{18A_{22}}{b^4} + \frac{A_{66}+2A_{12}}{a^2b^2}\right] + w_0^2\left[-\frac{6D_{11}}{a^4} + \frac{18D_{22}}{b^4} + \frac{D_{66}+2D_{12}}{a^2b^2}\right]. \tag{13b}$$

The critical energy release rate G_c controls the growth of the delamination. The propagation will stop when G drops below G_c. Since both G^a and G^b are decreasing with the growth of the delamination, crack propagation will eventually stop unless the central deflection w_0 approaches infinity. The penetration of composite laminates by sharp projectiles usually leaves a localized delamination region, since the sublaminate cannot deform very much before it is perforated.

Using the principle of Castigliano, the force of the sublaminate to resist penetration can be written as

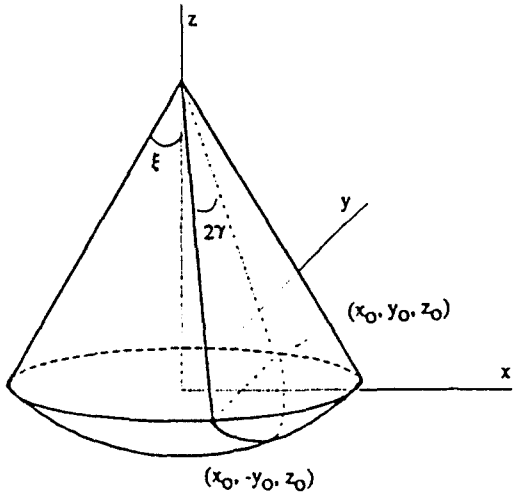

Fig. 3. A geodesic due to fiber deformation around the surface of a sphere.

$$P_0 = \frac{\partial U}{\partial w_0} = \frac{8\pi w_0^3 ab}{81}\left[\frac{6A_{11}}{a^4} + \frac{6A_{22}}{b^4} + \frac{A_{66}+2A_{12}}{a^2b^2}\right] + 2\pi w_0 ab\left[\frac{6D_{11}}{a^4} + \frac{6D_{22}}{b^4} + \frac{D_{66}+2D_{12}}{a^2b_2}\right]. \quad (14)$$

When the maximum resistance of the sublaminate is known, w_0 can be calculated from eqn (14).

In the present case of a circular delamination, the energy release rate reduces to

$$G_1 = \frac{2w_0^4}{81a^4}[18A_{11} - 6A_{22} + A_{66} + 2A_{12}] + \frac{w_0^2}{a^4}[18D_{11} - 6D_{22} + D_{66} + 2D_{12}]. \quad (15)$$

Similarly, eqn (14) can be expressed as

$$P = \frac{8\pi w_0^3}{81a^2}[6A_{11} + 6A_{22} + A_{66} + 2A_{12}] + 2\pi\frac{w_0}{a^2}[6D_{11} + 6D_{22} + D_{66} + 2D_{12}]. \quad (16)$$

The maximum delamination can be calculated by substituting the critical energy release rate and the maximum resistance of the sublaminate into eqns (15) and (16). The maximum delamination and the maximum deflection of the sublaminate relative to the plate can be determined from these relations. From the static penetration of a single layer laminate and the fracture toughness test, Zhu *et al.* (1991), the maximum resistance is 756 N, and the fracture toughness is about 450 J m^{-2}. The latter has been found to be only slightly dependent on strain rate, Saghizadh and Dharan (1986). By substituting these values into the above equations, the maximum delamination is obtained as 19.5 mm which is about three times the radius of the projectile. This is in agreement with the measured crack length.

(c) *Fiber deformation*

The extension of the fibers in front of the projectile results from both local and global target deformation; the corresponding strain is equal to the sum of the strains due to these two effects. The strain due to global deformation can be calculated from the strain–displacement relations of linear elasticity when the displacement field of the laminate is known. However, the local deformation of the fibers depends on their position. The strands not in contact with the cone are deformed due to bulging, while the fibers in contact are deformed around the indenter. When calculating the local fiber deformation, it is assumed that the composite is already delaminated. Thus, the fibers are not subjected to interlaminar constraint and form geodesic curves either on the surfaces of the indenter or on the spherical bulge, depending on their original locations and the instantaneous position of the penetrator tip.

For fiber deformation due to bulging, consider a fiber initially in the x–y plane which starts at point $(x_0 y_0, 0)$ and is deformed to terminate at point $(x_0, -y_0, 0)$ as shown in Fig. 3, with an initial length of $2y_0$. The geodesic on the surface of the sphere is a portion of a great circle. Therefore, the length of the deformed fiber is given by

$$l = 2r_n\gamma \quad (17)$$

where γ is the half angle of the sector of the great circle, and r_n is the radius of the sphere. The angle γ is given by

$$\gamma = \sin^{-1}\left[\frac{y_0}{\sqrt{x_0^2+y_0^2}}\sin\xi\right] \quad (18)$$

where ξ is the half cone angle of the bulge. The strain in the fiber is

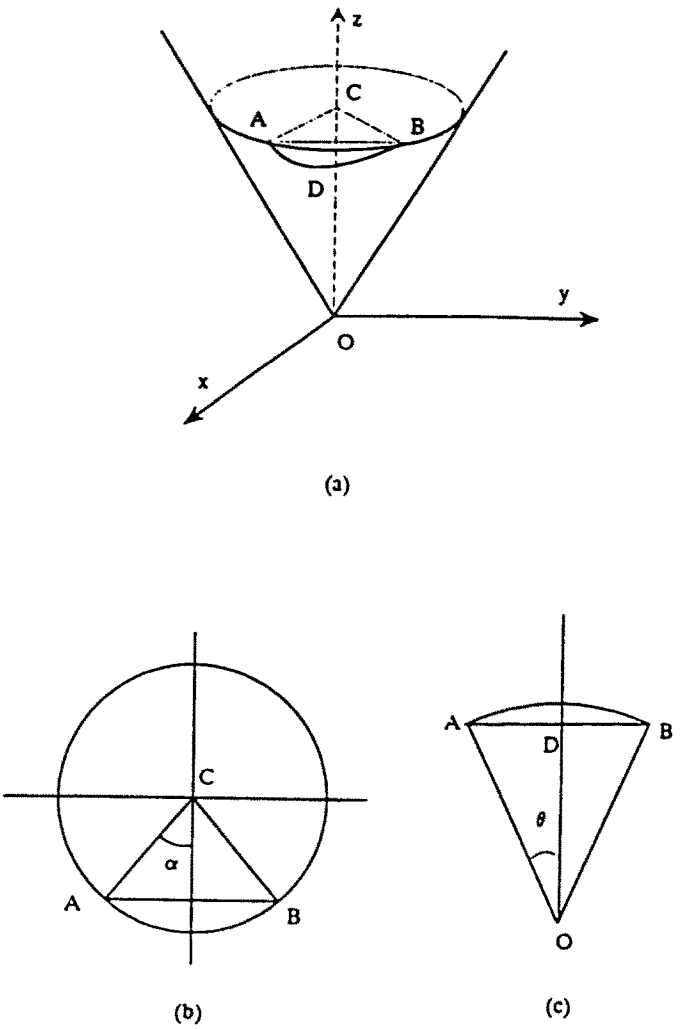

Fig. 4. A geodesic due to fiber deformation around the surface of a cone. (a) Coordinate system and location of fiber segment ADB on the surface of a cone; (b) Top view of conical section; (c) Developed cone surface.

$$\varepsilon_1 = \frac{l-2y_0}{2y_0} = \frac{\gamma}{\sin\gamma} - 1. \tag{19}$$

The ends of a fiber initially of length $2y_0$ in contact with the cone are (x_0, y_0, z_0) and $(x_0, -y_0, z_0)$, as shown in Fig. 4a. The equation of a cone surface in a coordinate frame whose origin is at its tip is

$$x^2 + y^2 = (z\tan\beta)^2 \tag{20}$$

where β is the half cone angle of the projectile.

The geodesic is a straight line in the developed surface of the cone. In order to calculate the length of the deformed fiber, the length of arc AB in plane ACB in Fig. 4b must be calculated. The half angle of ACB, α, is given by

$$\sin\alpha = \frac{y_0}{z_0\tan\beta}. \tag{21}$$

Therefore,

$$\text{arc } AB = (2z_0 \tan \beta)\alpha. \tag{22}$$

Arc AB forms part of a circle in the developed surface of the cone (Fig. 4c); length $\overline{ADB}$ is the length of the geodesic. The half angle θ of the sector developed from the cone surface is

$$\theta = \frac{\overline{AB}}{2\overline{OA}} = \alpha \sin \beta. \tag{23}$$

The length $\overline{ADB}$ can then be obtained from

$$\overline{ADB} = \frac{2z_0}{\cos \beta} \sin \theta \tag{24}$$

and the local strain in the fiber is

$$\varepsilon_l = \frac{\dfrac{z_0}{\cos \beta} \sin \left[\sin \beta \arcsin \left(\dfrac{y_0}{z_0 \tan \beta} \right) \right] - y_0}{y_0}. \tag{25}$$

The total strain in the fiber is

$$\varepsilon_f = \varepsilon_g + \varepsilon_l \tag{26}$$

where ε_g and ε_l represent the strains due to the global and local deformation, respectively. The maximum strain criterion is employed to determine fiber failure.

RESISTANCE TO PENETRATION

The force acting on the projectile is now calculated for the three stages of its motion.

(a) *Indentation*

The effects of the boundaries during indentation are neglected, a hypothesis which ignores the concurrent phenomena produced on the distal side. However, this representation is acceptable if the depth of the indentation is small relative to the plate thickness. For isotropic plates, it has been proposed that penetration is resisted by a uniform pressure p_m which, for a conical indenter provides the expression for the resistive force as, Tabor (1951),

$$F = p_m A_p = p_m \pi w_r^2 \tan^2 \beta \tag{27}$$

where p_m is the mean pressure, A_p is the projected contact area, and w_r is the indentation. It was also shown that the mean pressure was proportional to the yield stress σ_Y of the material, i.e.

$$p_m = c\sigma_Y. \tag{28}$$

This model is applied to the composite laminate. The mean pressure is obtained from static indentation experiments, Zhu *et al.* (1991). However, the direct extension of eqns (27) and (28) to the dynamic case neglects the strain rate effect. A simple way to take this effect into account for the present targets is to change the yield stress to a dynamic value using drop tests or Hopkinson-bar experiments, Zhu *et al.* (1991).

The indentation stage is terminated when fiber failure first occurs on the distal side of the target.

(b) *Perforation*

In this phase, further penetration increases the contact area and hence the resistance of the laminate, while, on the other hand, successive fiber failure reduces this resistance. A factor is introduced to approximate the effect of the material damage on the resistance, although this force cannot be specified directly. It was shown, Zhu *et al.* (1991), that fiber failure dominates the resistance of composites. Therefore, a damage factor, d_m, is chosen as

$$d_m = \frac{N_b}{N_t} \tag{29}$$

where N_b is the number of broken fibers, and N_t is the total number of unbroken fibers in front of the contact region. This factor is a function of time or indentation. The basic concept for this approach implies that the reduction in resistance is proportional to the number of failed fibers no matter where they are located. The resistance is expressed as

$$F = p_m A_p (1 - d_m) = p_m A_p \left(1 - \frac{N_b}{N_t}\right) \tag{30}$$

where A_p is the projected contact area between the laminate and the projectile. The number of broken fibers can be calculated from the proposed model of fiber deformation.

(c) *Exit of the projectile*

In the exit stage, friction is the only resistance to further motion of the projectile. Due to lack of information about dynamic friction, the average value obtained from the static penetration was used in the computation for the striker perforation. The exit stage starts when

$$F = F_\mu \tag{31}$$

where F_μ is the friction force measured during the static tests. This stage terminates when the projectile shank has completely separated from the target or when its velocity becomes zero.

RESULTS AND DISCUSSION

The relations describing the motion of the projectile during the three phases of the perforation process of a clamped plate were solved numerically for a 0/90 lay-up using a central finite difference scheme and subsequent smoothing by means of a spline fit, Zhu (1990). While the plate was circular, the influence of the boundary on the local deformation and damage is minimal, and hence each laminate was taken here to be clamped on a square boundary to simplify the computations. Symmetry of the system required the evaluation of the response for only one quarter of the plate. The target was initially quiescent and undeformed, and its middle surface was coincident with the x-y coordinate plane. The relevant system parameters required for this calculation are presented in Table 1.

Table 1. Computational parameters

In-plane tensile elastic modulus of laminate	6.9 GPa
In-plane Poisson's ratio	0.25
In-plane shear modulus	648 MPa
Out-of-plane shear modulus	338 MPa
Laminate density	1,230 kg m^{-3}
Mean pressure of indentation P_m	261 MPa
Friction force F_μ	1,068 N
Bullet mass	28.9 g
Bullet diameter	12.7 mm
Bullet length	38.1 mm
Tip cone angle	60°

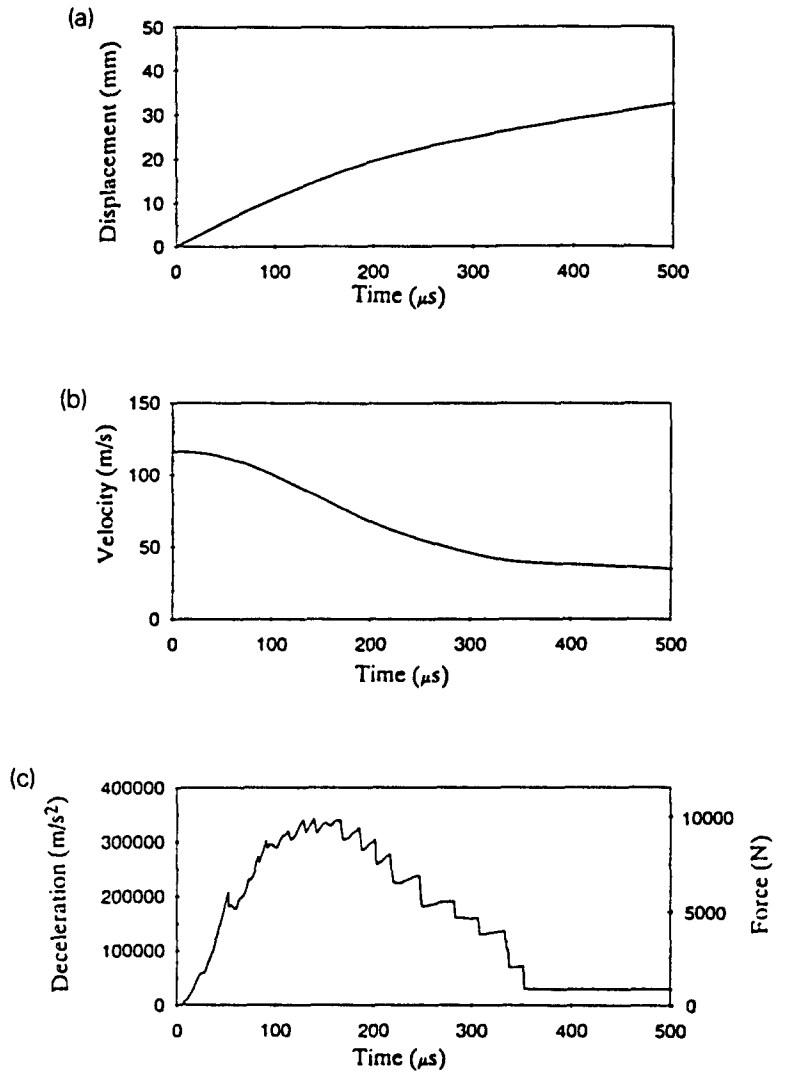

Fig. 5. Computed kinematic history of a 12.7 mm projectile with a 60° conical tip during penetration of a 10-ply Kevlar/polyester laminate at an initial velocity of 116 m s^{-1}. (a) Displacement; (b) Velocity; (c) Deceleration.

Figures 5 and 6 portray the computed kinematic history of the 60° cylindro-conical projectile perforating a 10-ply laminate at initial velocities of 116 m s^{-1} (ballistic limit) and 200 m s^{-1}, respectively. The peak deceleration is the same, 35×10^4 m s^{-2}, for these cases, but the duration for initial perforation is reduced from about 350 to 90 μs. The deceleration is maintained at a constant value corresponding to the friction force after the primary deceleration pulse has ended; it drops to zero upon complete separation of projectile and target. The oscillations in this pulse are due to successive fiber failures.

The effect of strain rate on the complex failure modalities cannot be ascertained exactly; limited quantitative information concerning through-thickness behavior is described by Zhu *et al.* (1991). A computation of the effect of strain rate on terminal velocity for 10-ply targets, obtained by increasing the static yield stress, and hence mean pressure, by 10% is shown in Fig. 7. A value of 6.9 MPa for the tensile Young's modulus was generally used in the computations; the effect of its variation on the terminal projectile velocity is shown in Fig. 8. The deviation due to each of these permutations is a maximum of 10% at the ballistic limit and substantially less with increasing velocity. Computations investigating the effect of lay-up on the terminal velocity showed negligible difference between 0/90 and 0/90/±45 laminates.

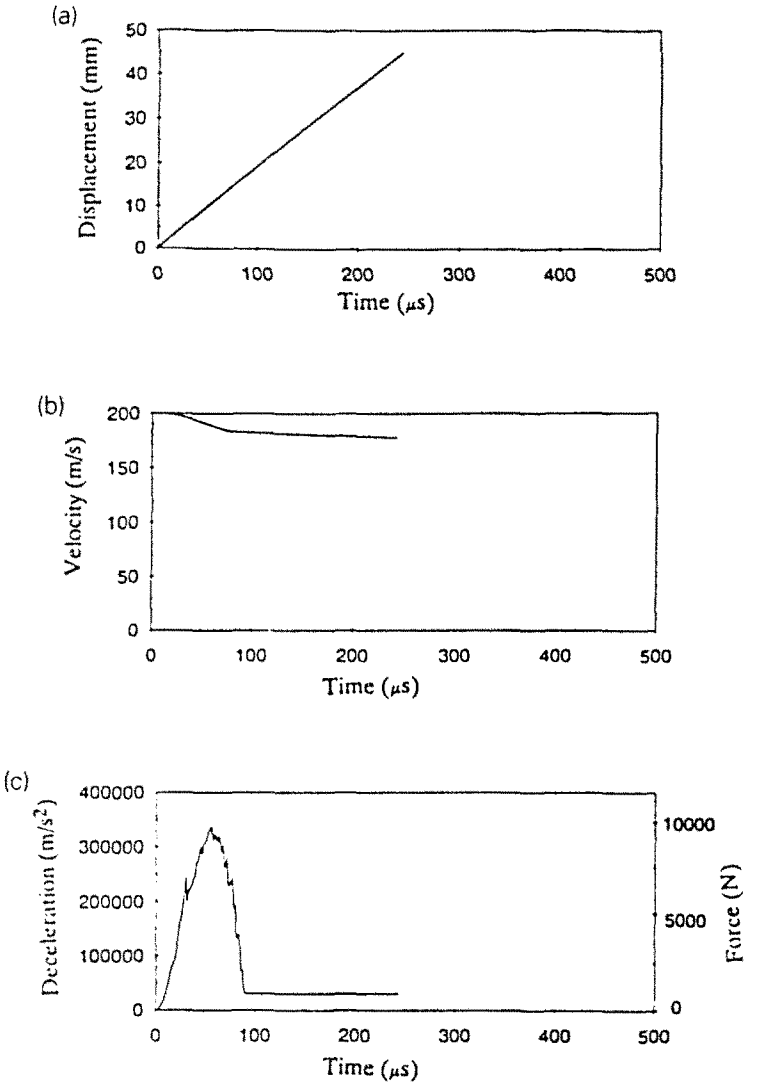

Fig. 6. Computer results for the conditions of Fig. 5 at an initial velocity of 200 m s^{-1}. (a) Displacement; (b) Velocity; (c) Deceleration.

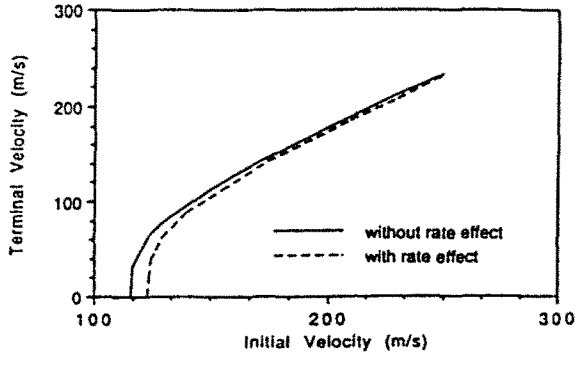

Fig. 7. Comparison of computed terminal velocities for a mean indentation pressure based on static values and one increased by 10% to simulate a strain rate effect.

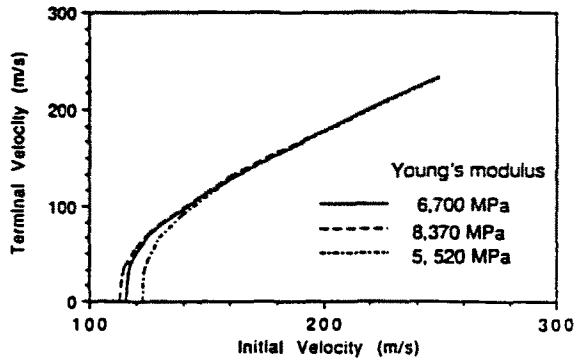

Fig. 8. Sensitivity of the computed terminal velocities to the value of the in-plane tensile Young's modulus. A value of 6.7 GPa was used in the general calculations.

The computed results for the ballistic limit of targets of various thicknesses are compared with data from experiments in Table 2 and Fig. 9, and very good agreement is noted in view of the complexity of the model. Corresponding information above the ballistic limit of 10-ply plates is presented in Fig. 10. The final projectile velocities for the laminates are somewhat overpredicted. One reason for the discrepancy may be the assumption involved in the description of the bulging process. Since an appropriate phenomenological model of this deformation cannot be obtained, a spherical shape was specified on the basis of observation. Such a configuration results in a state of uniform strain, and a discontinuity in strain was then required between the bulge and the exterior region. This condition resulted in early first fiber breakage, since fiber deformation along a spherical surface

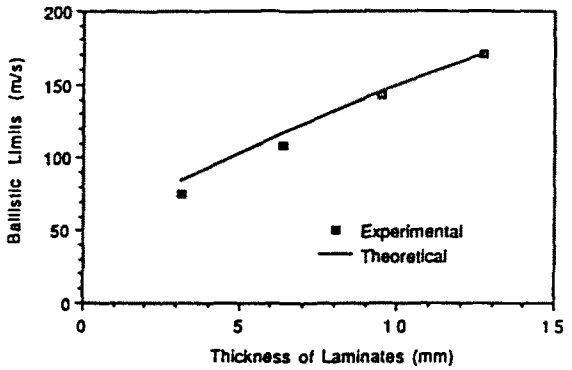

Fig. 9. Comparison of the ballistic limits for Kevlar/polyester laminates perforated by 12.7 mm diameter 60° cylindro-conical projectiles.

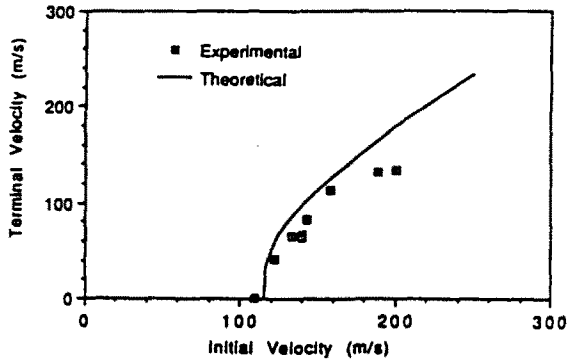

Fig. 10. Comparison of the terminal velocities for 10-ply Kevlar/polyester laminates perforated by 12.7 mm 60° cylindro-conical projectiles.

Table 2. Theoretical prediction of ballistic limits for Kevlar polyester laminates

Thickness of laminates (mm)	Number of plies	Experimental results (m s^{-1})	Theoretical prediction (m s^{-1})
3.125	5	75	84
6.35	10	109	116
9.525	15	143.2	145
12.7	20	170	170

produces a greater strain than when extended transversely by a sharp tip to the same deflection. Initial fiber failure was observed to occur on the distal side of the target in static tests and this situation is presumed to apply in the dynamic case as well.

The first fiber failure is the result of global deflection of the laminate and bulging. The maximum strain to failure of a Kevlar fiber is 4%, Lubin (1982). From the computation for a 10-ply laminate penetrated by a projectile at the ballistic limit, the strain due to the global deformation is about 1.9%, and the strain from bulging is 2.1%. This indicates that local and global deformation are of equal importance for cylindro-conical projectiles when the initial velocity of the striker is near the ballistic limit and that the corresponding strains are not negligible.

A comparison of the calculated and measured displacement, velocity and deceleration for a projectile with an initial velocity of 124 m s^{-1} penetrating a 10-ply target is presented in Fig. 11. The experimental values of the velocity and acceleration are obtained by

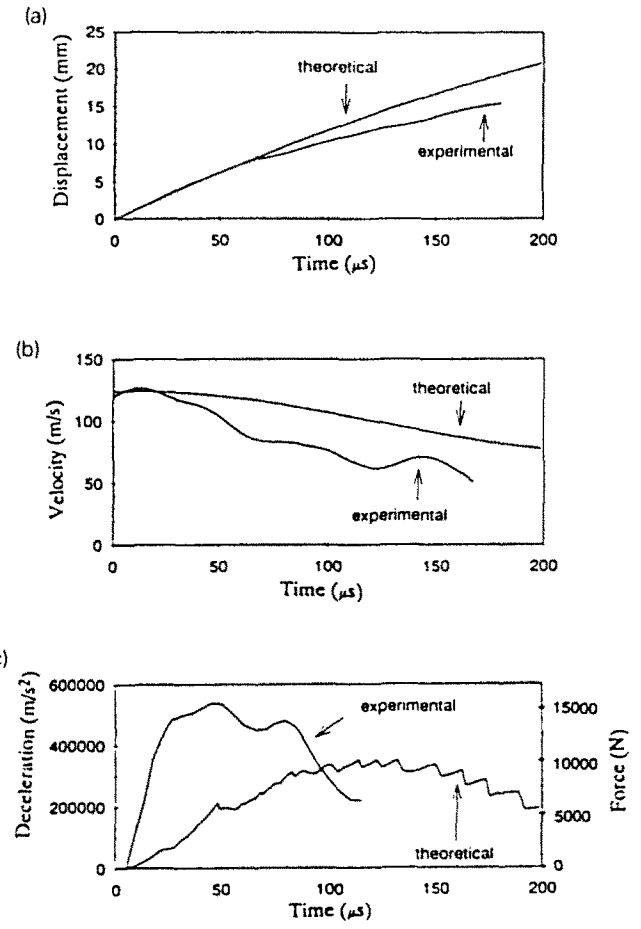

Fig. 11. Comparison of the calculated and measured kinematic histories of a 12.7 mm 60° cylindro-conical projectile during the perforation of a 10-ply Kevlar polyester laminate at an initial velocity of 124 m s^{-1}. (a) Displacement; (b) Velocity; (c) Deceleration.

successive differentiation of the position data; they exhibit increasing divergence from the analytical prediction, in part due to the inaccuracies inherent in the differentiation process. In addition, the raw data from the camera exhibit a certain degree of noise that has to be eliminated by smoothing. The predictions of the analysis are based on a host of simplifying assumptions and neglect of certain processes. This includes the use of linear theories, neglect of wave propagation, a solid friction model and neglect of the effect of this mechanism during the indentation process, and fiber breakage by the tip of the projectile rather than excessive elongation. In addition, the bulging model employed should be improved, and delamination due to bulging and large deformation rather than indentation alone should be incorporated. The most dramatic step in the improvement of the model is considered to be the inclusion of the strain rate effect in the indentation and global deformation description.

Forces are obtained from projectile acceleration histories using Newton's law. In Fig. 11, the peak experimental dynamic force value is 15 kN, compared with 13 kN obtained for similar quasi-static perforation. The corresponding model prediction is 10 kN, and the peak force here occurs substantially later than for the corresponding test results. These discrepancies may be improved by inclusion of the strain rate effect in a general theory of the process.

The peak deceleration detected by the OPTFOLLOW occurs at about 50 μs and the corresponding displacement is 6 mm. Thus, the mean pressure during dynamic indentation is 400 MPa, if the deflection of the plate is omitted, i.e. if w_0 is taken as zero. This value is 1.5 times the value of 261 MPa, the pressure in the quasistatic case. The length of the projectile tip is 11 mm and the thickness of the plate is 6.35 mm. Therefore, the maximum resistance of the laminate is reached before the projectile perforates the target.

The results also show that the tip of the projectile touched the distal surface of the target when the first fiber failed. If this was used as a criterion for the termination of the indentation stage, the maximum resistive force of the laminate from computation would be in better agreement with the experimental data.

SUMMARY AND CONCLUSIONS

A phenomenological model of the normal impact on laminated Kevlar/polyester plates of hard-steel cylindro-conical projectiles has been developed involving three successive stages of penetration: indentation, perforation and exit. The analysis comprised both global and local deformation, the former employing linearly elastic laminated plate theory, while the latter consisted of the indenting of the striker, bulging at the distal surface, fiber failure and delamination. Friction, neglected in the first two stages, was the only force acting during the exit phase. Resistance to the impingement of the striker was obtained from these dissipative mechanisms and used in conjunction with Newton's law to determine the response of the system.

A finite-difference computer program was developed to implement the computations using material properties either measured during the investigation or obtained from the literature. The results were compared with experimental data acquired in a parallel study.

It is concluded that the model provides a reasonable representation of the deformation and dissipative processes during penetration by a sharp-tipped rigid cylinder of relatively small aspect ratio. This is supported by the excellent accord between predictions and data for the ballistic limit of these plates, and for terminal velocities above this range. An increase in the constant value of the indentation pressure by 10%, presumed to simulate a strain-rate effect, resulted in a significant difference of the terminal velocity only in the vicinity of the ballistic limit, as was also the case for a change of 20% in the value of Young's modulus, used in the determination of the global deformation. Better agreement of the results of the model with test data is expected if bulging can be described analytically rather than by hypothesis and if a viscous representation for the target were to be employed throughout.

REFERENCES

Awerbuch, J. and Bodner, S. R. (1974). Analysis of the mechanics of penetration of projectiles in metallic plates. *Int. J. Solids Structures* **10**, 671–684.

Cairns, D. S. and Lagace, P. A. (1987). Thick composite plates subjected to lateral loading. *J. Appl. Mech.* **54**, 611–616.

Chai, H. (1982). The growth of impact damage in compressively loaded laminates. Ph.D. Dissertation, California Institute of Technology.

Chai, H. and Babcock, C. D. (1985). Two-dimensional modelling of compressive failure in delaminated laminates. *J. Comp. Mater.* **19**, 67–98.

Cristescu, N., Malvern, L. E. and Sierakowski, R. L. (1975). Failure mechanisms in composite plates impacted by blunt-ended penetrators. In *Foreign Object Impact Damage to Composites* (Edited by L. B. Greszczuk), pp. 159–172. ASTM STP 568, American Society for Testing and Materials, Philadelphia.

Dharan, C. K. H. (1978). Fracture mechanics of composite materials. *J. Engng Mater. Tech.* **100**, 233–247.

Dobyns, A. L. (1981). Analysis of simply-supported orthotropic plates subjected to static and dynamic loads. *AIAA Jl* **19**, 642–650.

Flanagan, F. (1988). Two-dimensional delamination growth in composite laminates under compression loading. In *Composite Materials: Testing and Design*, Eighth Conference (Edited by J. D. Whitcomb), pp. 180–190. ASTM STP 972, American Society for Testing and Materials, Philadelphia.

Garg, A. C. (1988). Delamination—a damage mode in composite structures. *Engng Frac. Mech.* **29**, 557–584.

Grady, J. E. and Sun, C. T. (1985). Dynamic delamination crack propagation in a graphite epoxy laminate. In *Composite Materials: Fatigue and Fracture* (Edited by H. T. Hahn), pp. 336–348. ASTM STP 907, American Society for Testing and Materials, Philadelphia.

Greszczuk, L. B. (1975). Response of isotropic and composite materials to particle impact. In *Foreign Object Impact Damage to Composites* (Edited by L. B. Greszczuk), pp. 183–211. ASTM STP 568, Americal Society for Testing and Materials, Philadelphia.

Greszczuk, L. B. and Chao, H. (1977). Impact damage in graphite-fiber reinforced composites. In *Composite Materials: Testing and Design*, Fourth Conference, pp. 389–408. ASTM STP 617, American Society for Testing and Materials, Philadelphia.

Reddy, J. N. (1982). Impact on laminated composite plates: a review of recent developments. In *Computational Aspects of Penetration Mechanics* (Edited by J. E. Flaherty), pp. 63–82. Lecture Notes in Engineering, **3**, Springer-Verlag, New York.

Saghizadeh, H. and Dharan, C. K. H. (1986). Delamination fracture toughness of graphite and aramid epoxy composites. *J. Engng Mater. Tech.* **108**, 290–295.

Shivakumar, K. N., Elber, W. and Illg, W. (1985a). Prediction of impact force and duration due to low-velocity impact on circular composite laminates. *J. Appl. Mech.* **52**, 674–680.

Shivakumar, K. N., Elber, W. and Illg, W. (1985b). Prediction of low-velocity impact damage in thin circular laminates. *AIAA Jl* **23**, 442–449.

Sun, C. T. (1977). An analytical method for evaluation of impact damage of laminated composites. In *Composite Materials: Testing and Design*, Fourth Conference, pp. 427–440. ASTM STP 617, American Society for Testing and Materials, Philadelphia.

Tabor, D. (1951). *The Hardness of Metals*. Clarendon Press, Oxford.

Tan, T. M. and Sun, C. T. (1985). Use of statical indentation laws in the impact analysis of laminated composite plates. *J. Appl. Mech.* **52**, 6–12.

Timoshenko, S. P. (1959). *Theory of Plates and Shells*. McGraw-Hill, New York.

Tsai, S. W. and Wu, E. M. (1971). A general theory of strength for anisotropic materials. *J. Comp. Mater.* **5**, 58–80.

Wang, A. S. D. (1984). Fracture mechanics of sublaminate cracks in composite materials. *Comp. Tech. Rev.* **6**, 45–62.

Whitney, J. M. and Pagano, N. J. (1970). Shear deformation in heterogeneous anisotropic plates. *J. Appl. Mech.* **37**, 1031–1036.

Wu, H.-Y. T. and Springer, G. S. (1988a). Measurements of matrix cracking and delamination caused by impact on composite plates. *J. Comp. Mater.* **22**, 518–532.

Wu, H.-Y. T. and Springer, G. S. (1988b). Impact induced stresses, strains and delamination in composite plates. *J. Comp. Mater.* **22**, 533–560.

Yang, P. C., Norris, C. H. and Stavsky, Y. (1966). Elastic wave propagation in heterogeneous plates. *Int. J. Solids Structures* **2**, 665–684.

Zhu, G. (1990). Penetration of laminated composites by projectiles. Ph.D. Dissertation, University of California, Berkeley.

Zhu, G., Goldsmith, W. and Dharan, C. K. H. (1991). Penetration of laminated Kevlar by projectiles—I. Experimental investigation. *Int. J. Solids Structures* **29**, 399–420.